

Impact of the chaotic semiconductor laser output power on time-delay-signature of chaos and random bit generation

Chenpeng Xue(薛琛鹏), Wang Xu(王绪), Likai Zheng(郑利凯), Haoyu Zhang(张昊宇), Yanhua Hong, and Zuxing Zhang(张祖兴)

Citation: Chin. Phys. B, 2025, 34 (**3**): 030504. DOI: 10.1088/1674-1056/ada7dd
Journal homepage: http://cpb.iphy.ac.cn; http://iopscience.iop.org/cpb

What follows is a list of articles you may be interested in

A fractional-order chaotic Lorenz-based chemical system: Dynamic investigation, complexity analysis, chaos synchronization, and its application to secure communication

Haneche Nabil and Hamaizia Tayeb
Chin. Phys. B, 2024, 33 (**12**): 120503. DOI: 10.1088/1674-1056/ad7fcf

Dynamical analysis, control, boundedness, and prediction for a fractional-order financial risk system

Kehao Yang(杨轲皓), Song Zheng(郑松), Tianhu Yu(余天虎), Aceng Sambas, Muhamad Deni Johansyah, Hassan Saberi-Nik, and Mohamad Afendee Mohamed
Chin. Phys. B, 2024, 33 (**11**): 110501. DOI: 10.1088/1674-1056/ad7afb

Remote sensing image encryption algorithm based on novel hyperchaos and an elliptic curve cryptosystem

Jing-Xi Tian(田婧希), Song-Chang Jin(金松昌), Xiao-Qiang Zhang(张晓强), Shao-Wu Yang(杨绍武), and Dian-Xi Shi(史殿习)
Chin. Phys. B, 2024, 33 (**5**): 050502. DOI: 10.1088/1674-1056/ad20d9

Coexistence behavior of asymmetric attractors in hyperbolic-type memristive Hopfield neural network and its application in image encryption

Xiaoxia Li(李晓霞), Qianqian He(何倩倩), Tianyi Yu(余天意),Zhuang Cai(才壮), and Guizhi Xu(徐桂芝)
Chin. Phys. B, 2024, 33 (**3**): 030505. DOI: 10.1088/1674-1056/acf281

A novel variable-order fractional chaotic map and its dynamics

Zhouqing Tang(唐周青), Shaobo He(贺少波), Huihai Wang(王会海), Kehui Sun(孙克辉), Zhao Yao(姚昭), and Xianming Wu(吴先明)
Chin. Phys. B, 2024, 33 (**3**): 030503. DOI: 10.1088/1674-1056/ad1a93

Impact of the chaotic semiconductor laser output power on time-delay-signature of chaos and random bit generation

Chenpeng Xue(薛琛鹏)[1], Xu Wang(王绪)[1], Likai Zheng(郑利凯)[1], Haoyu Zhang(张昊宇)[1], Yanhua Hong[2], and Zuxing Zhang(张祖兴)[1,†]

[1] *College of Electronic and Optical Engineering and College of Flexible Electronics (Future Technology), Nanjing University of Posts and Telecommunications, Nanjing* 210023, *China*

[2] *School of Computer Science and Engineering, Bangor University, Bangor LL57 1UT, UK*

(Received 3 December 2024; revised manuscript received 5 January 2025; accepted manuscript online 9 January 2025)

We experimentally analyze the effect of the optical power on the time delay signature identification and the random bit generation in chaotic semiconductor laser with optical feedback. Due to the inevitable noise during the photoelectric detection and analog-digital conversion, the varying of output optical power would change the signal to noise ratio, then impact time delay signature identification and the random bit generation. Our results show that, when the optical power is less than −14 dBm, with the decreasing of the optical power, the actual identified time delay signature degrades and the entropy of the chaotic signal increases. Moreover, the extracted random bit sequence with lower optical power is more easily pass through the randomness testing.

Keywords: chaos, time delay signature, entropy estimation, random bit generation

PACS: 05.45.–a, 05.45.Gg, 05.45.Tp, 05.40.Ca

DOI: 10.1088/1674-1056/ada7dd **CSTR:** 32038.14.CPB.ada7dd

1. Introduction

Optical chaos utilizing semiconductor laser (SL) have garnered significant attention since the potential application in secure communication, random bit generation, secure key distribution, lidar and sensor.[1–11] The external optical feedback can lead to high-dimensional chaos by introducing infinite degrees of freedom in semiconductor laser dynamics, which is desired for the aforementioned applications. Nevertheless, the deterministic feedback loop can give rise to the cycle dependency in the chaotic system corresponding to the time delay of the feedback round trip, namely, the time-delay signature (TDS). TDS can induce the reduction of the complexity and indeterminacy. Moreover, the time delay of feedback would also be leaked out since it can be estimated easily by the autocorrelation function (ACF), permutation entropy (PE), delayed mutual information (DMI), reservoir computing, convolutional neural network from the time series.[12–15] In short, the TDS is undesired for the random bit generation, secure communication and lidar.

Plenty of schemes for the TDS suppression of the chaotic system with optical feedback or optoelectronic feedback have been proposed.[16–19] Among them, one general approach is to modify the feedback loop. For instance, using an ultra-short external cavity with the delay time close to the relaxation-oscillation period, the TDS can be effectively suppressed under relatively weak feedback.[20] Dual feedback can also be used to suppress the TDS, by setting difference of delay time equaling to the relaxation-oscillation period.[21] TDS suppression under multi-path optical feedback is also experimentally demonstrated, where in no need of the precise control of cavity length.[22,23] Lately, optical feedback from a fiber Bragg gratings with a properly positive frequency detuning to the semiconductor laser can greatly suppress the TDS.[24] Optical with high dispersion in feedback loop is demonstrated can also significantly suppress the TDS.[25–27] Alternatively, there are other ways for the TDS suppression. For instance, Li *et al*. proposed a TDS suppression and bandwidth enhancement by using the anomalous group-velocity dispersion and self-phase modulation during the fiber propagation.[28] Zhao *et al*. proposed TDS suppression based on the generative adversarial network for post-processing.[29] However, few works focus on the condition of TDS estimation. Because of the inevitable thermal noise in the photoelectric detection and ADC processing, it is reasonable to deduce that the size of actual detected TDS would change with the varying of the output optical power and signal to noise ratio (SNR). Moreover as the TDS adversely affects the random bit generation, the random bit extraction versus the output optical power is also worth studying.

In this work, we experimentally verified with the drop of output optical power, the TDS embedded in chaotic time series is suppressed, the entropy of chaos increases and more low significant bits could be reserved for the high-speed physical random generation.

†Corresponding author. E-mail: zxzhang@njupt.edu.cn

© 2025 Chinese Physical Society and IOP Publishing Ltd. All rights, including for text and data mining, AI training, and similar technologies, are reserved.

2. Principle and experimental setup

Figure 1 illustrates the experimental setup of the chaotic semiconductor laser subject to a dispersion optical feedback by a chirped fiber Bragg grating (CFBG). The SL is driven by a low noise laser diode controller (Overlink, OULD-600B). The pump current is set at 30 mA (The threshold current of the laser is 5.86 mA) and the temperature is stabilized at 16.00 °C. The CFBG with dispersion coefficient of 870 ps/nm is used for the dispersion feedback. By properly adjusting the feedback power, the SL can work in the chaotic regime. The time series and power spectrum are measured by an 11-GHz serial data analyzer (LeCroy, SDA 11000) and a spectrum analyzer (Rohde and Schwarz, FSW) with a 40-GHz PIN photodetector (Overlink, PD-1000). The optical spectrum of the laser is measured by an optical spectrum analyzer (YOKOGAWA, AQ6370D) with a 0.02-nm resolution.

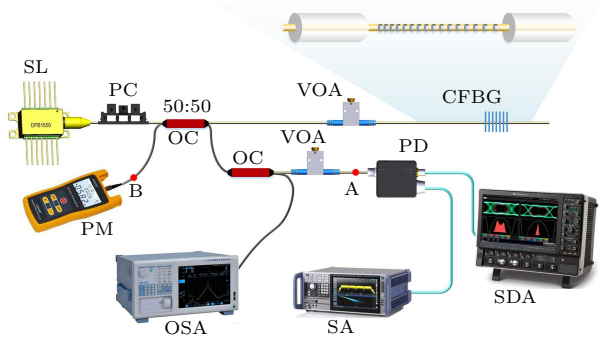


Fig. 1. Experimental setup. SL: semiconductor laser, PC: polarization controller, OC: optical coupler, VOA: variable optical attenuator, CFBG: chirped fiber Bragg grating, PD: photodetector, OSA: optical spectrum analyzer, SDA: serial data analyzer, SA: spectrum analyzer.

Figure 2(a) shows the reflectance spectrum of the CFBG and the optical spectrum of the chaotic SL with the CFBG feedback. The feedback power observed by the power meter (PM) is set at −9 dBm and the output optical power detected at point A is set at 1 dBm, which can be changed by the VOA. The CFBG hold a 3-dB bandwidth of ∼ 0.45 nm, and the wavelength of the SL is at the center of the reflection spectrum of the CFBG. Figure 2(b) displays the temporary waveforms of the SL with the CFBG feedback. Clearly, due to the optical feedback, the balance of carrier–photon interaction in the laser medium is broken and the output of SL presents the significant instability of intensity. Figure 2(c) displays the corresponding power spectrum. Here, the standard chaotic bandwidth BW_s defined as the maximum frequency including 80% of the total spectral power from the DC component,[30] and the effective chaotic bandwidth BW_e defined by summing up only those discrete spectral segments of the chaos power spectrum accounting for 80% of the total power,[31] are used to estimate the bandwidth. According to the power spectrum in Fig. 2(c), the BW_s and BW_e are about 16.61 GHz and 13.70 GHz respectively.

Next, the ACF and PE are adopted to estimate the TDS of chaos in this paper. The formula of ACF is formed as

$$C(\Delta t) = \frac{\langle (I(t) - \langle I(t)\rangle)\,(I(t+\Delta t) - \langle I(t+\Delta t)\rangle)\rangle}{\sigma_I^2}, \qquad (1)$$

where $I(t)$ is the intensity time-series, Δt is the lag time, $\langle\cdot\rangle$ denotes the time averaging, σ_I is the standard deviation of $I(t)$.

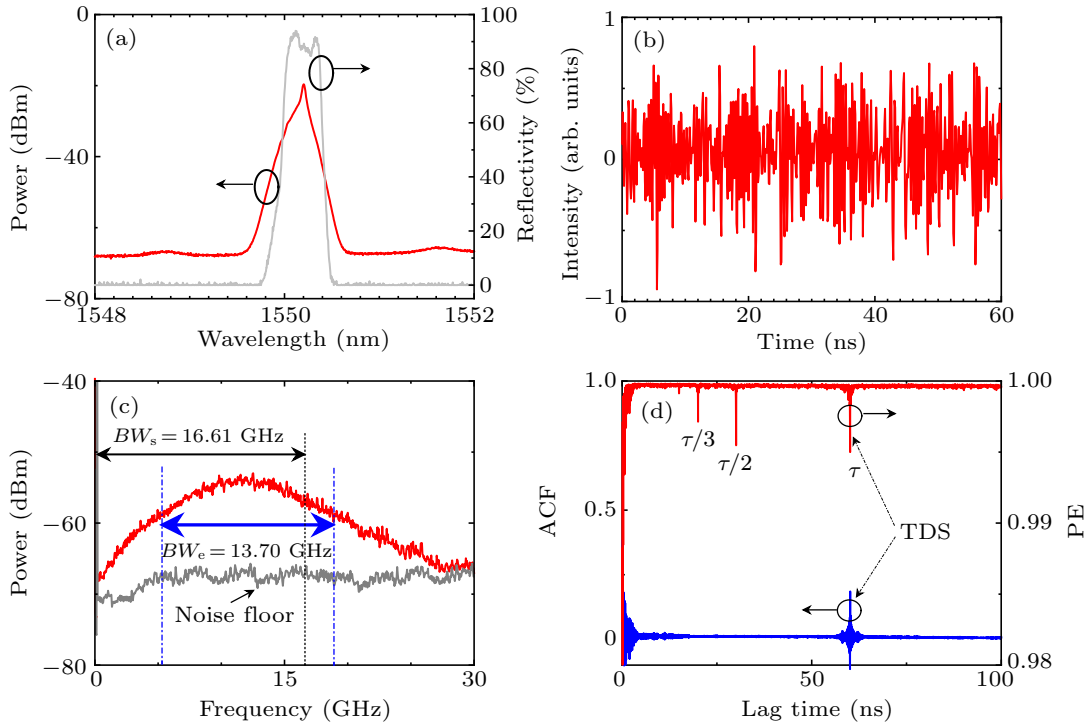


Fig. 2. Characteristics of the chaos in the SL subject to CFBG feedback, (a) optical spectrum (red), and reflectance spectrum of the CFBG (gray); (b) time-domain waveforms, (c) power spectrum, BW_s: standard bandwidth, BW_e: effective bandwidth, and (d) ACF and PE curves, $D = 5$, $N = 5 \times 10^4$.

As for the PE, given a time series $\{x_t, t = 1,2,\ldots,N\}$, an embedding dimension D, an embedding delay time τ_D, and $N \gg D!$, the set of order D can be given by $S = [x(t), x(t+\tau_D), \ldots, x(t+(D-1)\tau_D)]$. Then it can be arranged as $[x(t+(r_1-1)\tau_D), x(t+(r_2-1)\tau_D), \ldots, x(t+(r_D-1)\tau_D)]$ in the order of smallest to largest in size. When $x(t+(r_1-1)\tau_D) = x(t+(r_2-1)\tau_D)$, we arrange $x(t+(r_1-1)\tau_D)$ before $x(t+(r_2-1)\tau_D)$ if $r_1 < r_2$. Hence, any S can be uniquely mapped into an ordinal pattern $\Gamma = (r_1, r_2, \ldots, r_D)$, which is one of permutations of D distinct symbols (1, 2,..., D). For all the possible permutations, the probability distribution is given as

$$p(\Gamma) = \frac{\#\{t | t \le N - D + 1; S \text{ has type } \Gamma\}}{N - D + 1}, \tag{2}$$

where # stands for "number", then the PE is evaluated by

$$h(\mathrm{p}) = -\sum p(\Gamma) \log(p(\Gamma)). \tag{3}$$

Figure 2(d) shows the ACF and PE curves calculated from the intensity time series as a function of the lag time. Obviously, there are evident peak and trough (TDS) located at around $\tau = 60.15$ ns in the ACF and PE curves, which is also the time delay of the optical feedback loop. Moreover, we also observe troughs in PE at subharmonics of τ, e.g. $\tau/2$ and $\tau/3$.

Figure 3(a) shows the variance evolution of the chaotic intensity time series with respect to that of the measurement system noise versus the output optical power. With the increasing of the optical power, the variance ratio of chaos to noise firstly increases rapidly with increasing of optical power, which indicate a significant drop in the SNR. When the optical power is over −11 dBm, the variance ratio generally tends to be stable. This can be attributed to the automatic gain control adopted in the PD. The inset figures show the measurement system noise and the intensity time series with different output powers. Next, the impact of the output optical power on the detected TDS is studied. Here the TDS size is estimated by the prominences of maximum peak in the ACF curve and trough in the PE curve. Figure 3(b) shows the TDS sizes calculated by the ACF and PE. Apparently, when the optical power is over −11 dBm, the TDS size is around 0.15 identified by the ACF. With the further decreasing of the optical power, the TDS decreases gradually. For instance, when the optical power is −14 dBm, the TDS is about 0.10, when the optical power decreases to −20 dBm, the TDS is 0.08. This is due to the degraded of the SNR.[32] Similar evolution of PE versus the optical power is also observed. For instance, when the optical power is over 11 dBm, the TDS is about 0.0041. When the output power decreases to −14 dBm, the TDS is 0.0016. With the output power is −2 dBm, the calculated TDS is dropped to ∼ 0.0008.

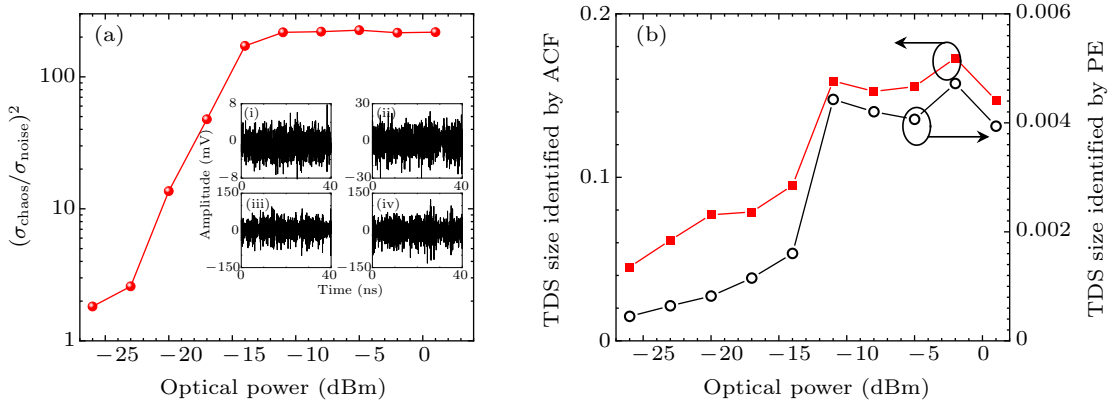


Fig. 3. Variance evolution of the chaotic intensity time series with respect to that of the measurement system noise and TDS size as a function of the optical power, (a) variance evolution and (b) TDS sizes identified by the ACF and PE, σ_{chaos} and σ_{noise} donated the standard deviation of chaos and the measurement system noise respectively. The inset figures show the waveforms (i) noise, (ii) −20 dBm, (iii) −14 dBm, and (iv) 1 dBm.

Then the random bit extraction from the chaos signal as a function of the optical output power is studied. The initial data acquired from the SDA 11000 with a sampling rate of 20 GSa/s is re-quantized with a resolution 8-bits in the Matlab. Here the vertical windows size of the temporal waveform is set at ±6 times its standard deviation to ensure the same 8-bits acquisition condition (from −127 to +127 in integer) for the cases with different optical powers. Firstly an entropy estimation is used to show the entropy evolution of the acquired electronic chaos. Figure 4(a) presents the results of the NIST entropy estimation with forty million samples.[33] When the optical power is less than −11 dBm, the H_{NIST} increases with the decreasing of the optical power evidently, due to the significant degradation of the SNR. To conveniently characterize the influence of the noise on entropy, we adopt the method described in Ref. [33] to calculate the NIST entropy of the measurement systems noise in term of the n-bit digitization at different optical power settings. The results are shown in Fig. 4(b). It is noted that with the decreasing of the optical powers, the entropy of the noise witnesses a significant increase, which leads to the entropy increasing of chaos as shown in Fig. 4(a). For the entropy estimation of chaos, the contribution of the noise is adverse. However, for the physical random bit generation, the entropy increase is desired since it determines the theoretical maximum speed of the permitted random bit. Therefore, properly setting the optical power is

suggested, especially for the high-bit resolution.

Next, the physical random bit extraction form the chaos with different optical powers is studied in filed. Here, the finally random bit is generated by using the post-processing of retaining the least significant bits (LSB) and performing delay bitwise XOR.[34] The randomness of the generated sequence was tested using the NIST 800-22 test suite, which consists of 15 tests. According to NIST standard, at a significance level of 0.01, the success percentage should be within the range of 0.99250±0.0094392, and the combined p-value should be greater than 0.0001. For simplicity, we firstly use a 100×1 Mbits sequence for the NIST 800-22 testing, and collect the number of passed tests. As shown in Fig. 5(a), for the 4LSB and 5LSB, all the 15 tests in the NIST test suite can be passed. While for the 6LSB, it can only pass the 15 tests when the optical power is not exceeding −14 dBm.

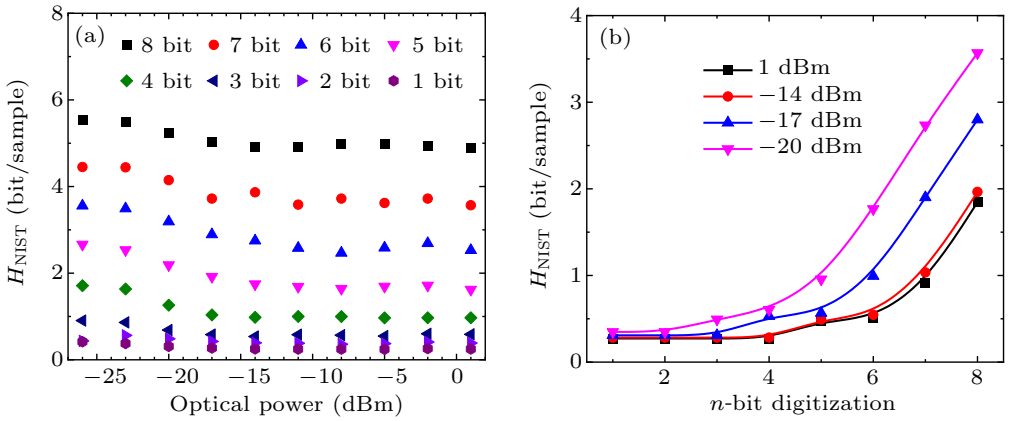


Fig. 4. (a) H_{NIST} of the chaos at different n as a function of optical power and (b) H_{NIST} of the noise in terms of n at different optical powers.

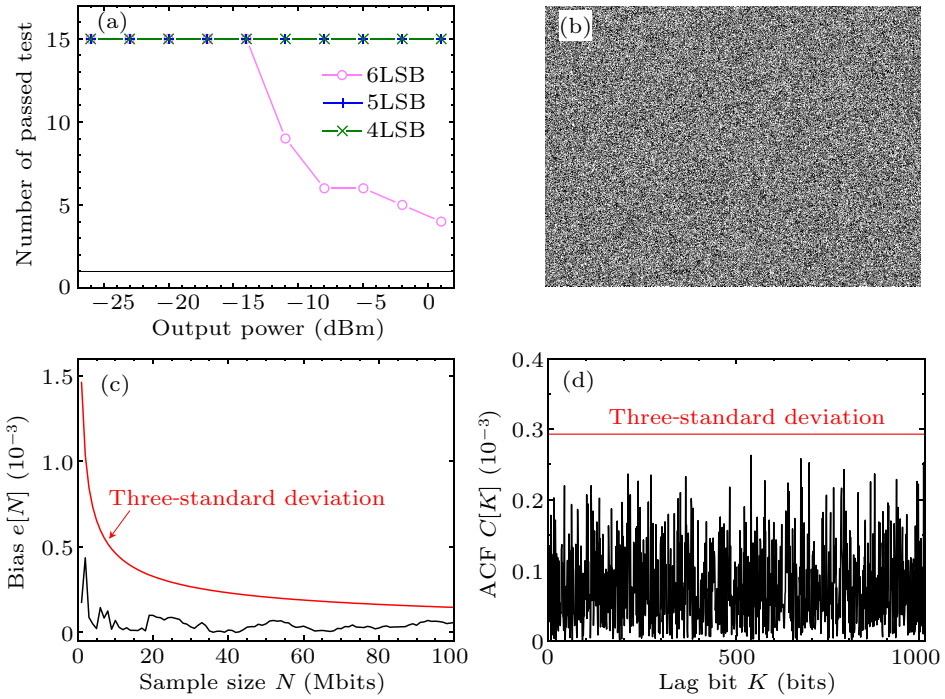


Fig. 5. (a) Number of pass tests with 100×1 Mbits samples versus the optical power, 4LSB is retaining the least significant 4 bits, 5LSB is retaining the least significant 5 bits, and 6LSB is retaining the least significant 6 bits for each sample. (b) Bitmap image constructed using 1000×1000 random bits: white ones denote '1' and black denote '0', (c) physical-random-number bias curves for sample size, (d) ACF as a function of delay bit K.

Figure 5(b) shows the bitmap image that constructed using 1000×1000 random bits of 6LSB retaining at −14 dBm, in which white ones denote '1' and black denote '0'. Clearly, no obvious black and white bias is observed, as well as no clear graphs of patterns or periodic shapes are shown, which indicates that the generated keys are qualitatively unbiased and internally independent. Moreover, we also qualitatively calculate the bias of the random bits $e[m]$ and the autocorrelation coefficient $C[K]$ of the random numbers,[4,35] which are expressed as follows:

$$e[m] = |\langle a[m]\rangle - 0.5|, \tag{4}$$

$$C[K] = \frac{\langle a[m]a[m+K]\rangle - \langle a[m]\rangle^2}{\langle a^2[m]\rangle - \langle a[m]\rangle^2}, \tag{5}$$

where $a[m]$, $a[m+K]$ are random sequences of m-bit length, K denotes the length of the delayed bit, and $\langle\cdot\rangle$ denotes the statistical average over m bits. Figure 5(c) shows the calculated biases as a function of the random sequences length m (from 1 Mbits to 100 Mbits). It is obvious that the biases always remain below the level of three standard deviations $3\sigma_{\text{bias}} = 1.5\ \text{m}^{-1}$, which indicates that the generated key is also unbiased in quantitative analysis. Figure 5(d) shows the autocorrelation (AC) function as a function of the bits of delay (the sample size is 100 Mbits). Similarly, the autocorrelation function has also been kept below the three standard deviation level $3\sigma_{\text{AC}} = 3\ \text{m}^{-1}$, which indicates that the random bit generated with 6LSB and -14 dBm is also internally independent in the quantitative analysis. In summary, we can conclude that the random bits extracted is unbiased and internally independent.

Figure 6 displays the results (1000 samples of 1 Mbits sequences) of the random bit generation with different LSBs retaining. Firstly, for random bits generation with 6LSB at -14 dBm, it can pass all the 15 NIST tests, which indicate that the random bits generated under the acquisition condition possesses strong randomness. When we increasing the output power to 1 dBm, the 4LSB and 5LSB can still pass the tests, while the 6LSB case fails.

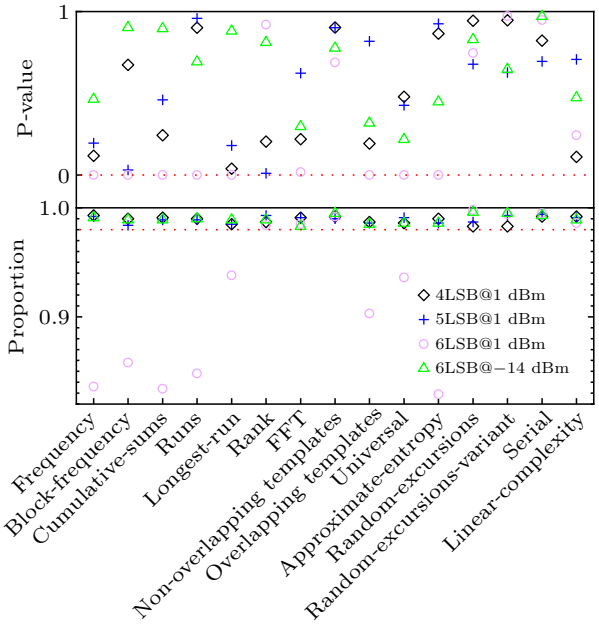


Fig. 6. Result of NIST 800-22 Test of random bits generation with different LSBs retaining and optical output power, 1000 samples of 1-Mbits sequences.

3. Conclusion

We have experimentally analyzed the effect of the optical power on the TDS identification and the random bit generation in chaotic semiconductor laser with optical feedback. A semiconductor laser subject dispersion feedback from a CFBG is used to generate the chaos. ACF, PE, and NIST entropy are used to estimate the TDS and entropy of the chaos. The TDS would degrease and NIST entropy would increase with the reducing of the optical power. For simplicity, only the measurement system noise is considered in this work. A study of the chaos variance to noise variance also presented the drop of the SNR with the decreasing of the optical power. We can easily deducted that the reducing in the optical power, would drop the SNR, and then to suppress the TDS and increase the entropy. Moreover, NIST 800-22 test suite is also used to test the generated random bit sequences. The results show that with the decreasing of the output optical power, the extracted random bit sequence is more easily passed through the randomness testing.

Acknowledgement

Project supported in part by the National Natural Science Foundation of China (Grant Nos. 62005129 and 62175116).

References

[1] Argyris A, Syvridis D, Larger L, Annovazzi-Lodi V, Colet P, Fischer I, García-Ojalvo J, Mirasso C R, Pesquera L and Shore K A 2005 *Nature* **438** 343
[2] Xiang S, Wang B, Wang Y, Han Y, Wen A and Hao Y 2019 *J. Lightw. Technol.* **37** 3987
[3] Gao H, Wang A, Wang L, Jia Z, Guo Y, Gao Z, Yan L, Qin Y and Wang Y 2021 *Light Sci. Appl.* **10** 172
[4] Li J, Li Y, Dong Y, Yang Y, Xiao J and Huang Y 2023 *Chin. Opt. Lett.* **21** 061901
[5] Cheng C H, Chen C Y, Chen J D, Pan D K, Ting K T and Lin F Y 2018 *Opt. Express* **26** 12230
[6] Gao Z, Li Q, Tang B, Zhang L, Luo Y, Fu S, Li Z, Wang Y and Qin Y 2022 *Conference on Lasers and Electro-Optics*, May 15–20, 2022, San Jose, California, USA, p. SF4L.4
[7] Wu Y, Luo H, Deng L, Yang Q, Dai X, liu D and Cheng M 2022 *Opt. Lett.* **47** 5285
[8] Yang Z, Yi L, Ke J, Zhuge Q, Yang Y and Hu W 2020 *J. Lightw. Technol.* **38** 4648
[9] Li P, Li Q, Tang W, Wang W, Zhang W, Little B E, Chu S T, Shore K A, Qin Y and Wang Y 2024 *Light Sci. Appl.* **13** 66
[10] Liu S, Jiang N, Zhang Y, Wang C, Zhao A, Qiu K and Zhang Q 2022 *Opt. Express* **30** 32366
[11] Wang C, Li J, Zhou X, Cheng Z, Qiao L, Xue X and Zhang M 2023 *Light Sci. Appl.* **12** 213
[12] Udaltsov V S, Larger L, Goedgebuer J P, Locquet A and Citrin D S 2005 *J. Opt. Technol.* **72** 373
[13] Kai C, Li P, Wang B, Shore K A, Qin Y and Wang Y 2023 *IEEE J. Sel. Top. Quantum Electron.* **29** 7700407
[14] Chen Y, Xin R, Cheng M, Gao X, Li S, Shao W, Deng L, Zhang M, Fu S and Liu D 2020 *Opt. Express* **28** 15221
[15] Zunino L, Soriano M C, Fischer I, Rosso O A and Mirasso C R 2010 *Phys. Rev. E* **82** 046212
[16] Rontani D, Locquet A, Sciamanna M, Citrin D S and Ortin S 2009 *IEEE J. Quantum Electron.* **45** 879
[17] Zhang J, Feng C, Zhang M, Liu Y, Wu C and Wang Y 2018 *Opt. Express* **26** 6962
[18] Wang Y, Xiang S, Wang B, Cao X, Wen A and Hao Y 2019 *Opt. Express* **27** 8446
[19] Jiang N, Wang Y, Zhao A, Liu S, Zhang Y, Chen L, Li B and Qiu K 2020 *Opt. Express* **28** 1999
[20] Rontani D, Locquet A, Sciamanna M and Citrin D S 2007 *Opt. Lett.* **32** 2960
[21] Wu J, Xia G and Wu Z 2009 *Opt. Express* **17** 20124

[22] Cui B, Xia G, Tang X, Wang F, Jiang Z, Zheng Y, Zhang F and Wu Z 2022 *IEEE Photon. J.* **14** 1504605
[23] Hong Y, Zhong Z and Shore K A 2024 *Frontiers in Network Physiology* **3** 1330375
[24] Li S S and Chan S C 2015 *IEEE J. Sel. Top. Quantum Electron.* **21** 1800812
[25] Ke J, Yi L, Hou T, Hu Y, Xia G and Hu W 2017 *IEEE Photon. J.* **9** 7200808
[26] Wang D, Wang L, Zhao T, Gao H, Wang Y, Chen X and Wang A 2017 *Opt. Express* **25** 10911
[27] Wang D, Lei Y, Shi P and Li Z 2023 *Chin. Phys. B* **32** 90505
[28] Li S S, Li X Z and Chan S C 2018 *Opt. Lett.* **43** 4751
[29] Zhao A, Jiang N, Wang C, Liu S and Qiu K 2023 *Acta Opt. Sin.* **43** 0114002
[30] Lin F Y and Liu J M 2003 *Opt. Commun.* **221** 173
[31] Lin, F Y, Chao Y K and Wu T C 2012 *IEEE J Quantum Electron.* **48** 1010
[32] Agrawal G P 2010 *Fiber-Optics Communication Systems*, 4th edn. (New York: Jhon Wiley & Sons) pp. 151–154
[33] Tseng C H, Funabashi R, Kanno K, Uchida A, Wei C C and Hwang S K 2024 *Opt. Express* **32** 23097
[34] Yamazaki T and Uchida A 2013 *IEEE J. Sel. Top. Quantum Electron.* **19** 0600309
[35] Guo H, Tang W, Liu Y and Wei W 2010 *Phys. Rev. E* **81** 051137